



Cite this: *Nanoscale*, 2018, **10**, 8329

## Resolving the optical anisotropy of low-symmetry 2D materials†

Wanfu Shen,<sup>a</sup> Chunguang Hu,<sup>a</sup> Jin Tao,<sup>b</sup> Jun Liu,<sup>a</sup> Shuangqing Fan,<sup>a</sup> Yaxu Wei,<sup>a</sup> Chunhua An,<sup>a</sup> Jiancui Chen,<sup>a</sup> Sen Wu,<sup>a</sup> Yanning Li,<sup>a</sup> Jing Liu,<sup>a</sup> Daihua Zhang,<sup>a</sup> Lidong Sun<sup>c</sup> and Xiaotang Hu<sup>a</sup>

Optical anisotropy is one of the most fundamental physical characteristics of emerging low-symmetry two-dimensional (2D) materials. It provides abundant structural information and is crucial for creating diverse nanoscale devices. Here, we have proposed an azimuth-resolved microscopic approach to directly resolve the normalized optical difference along two orthogonal directions at normal incidence. The differential principle ensures that the approach is only sensitive to anisotropic samples and immune to isotropic materials. We studied the optical anisotropy of bare and encapsulated black phosphorus (BP) and unveiled the interference effect on optical anisotropy, which is critical for practical applications in optical and optoelectronic devices. A multi-phase model based on the scattering matrix method was developed to account for the interference effect and then the crystallographic directions were unambiguously determined. Our result also suggests that the optical anisotropy is a probe to measure the thickness with monolayer resolution. Furthermore, the optical anisotropy of rhenium disulfide (ReS<sub>2</sub>), another class of anisotropic 2D materials, with a 1T distorted crystal structure, was investigated, which demonstrates that our approach is suitable for other anisotropic 2D materials. This technique is ideal for optical anisotropy characterization and will inspire future efforts in BP and related anisotropic 2D nanomaterials for engineering new conceptual nanodevices.

Received 10th December 2017,  
Accepted 26th March 2018

DOI: 10.1039/c7nr09173g

rsc.li/nanoscale

## Introduction

Low-symmetry two-dimensional (2D) materials, such as black phosphorus (BP),<sup>1–5</sup> rhenium disulfide (ReS<sub>2</sub>) and<sup>6–8</sup> tungsten ditelluride (WTe<sub>2</sub>),<sup>9,10</sup> are emerging as new members of the family of 2D materials. These materials not only possess merits comparable to those of the most studied isotropic graphene<sup>11,12</sup> and 2D transition metal dichalcogenides (TMDs),<sup>13</sup> such as high mobility and a large on/off ratio, but also exhibit unique in-plane electrical, optical, and thermal anisotropy due to their asymmetrical crystalline structure.<sup>1–4,6,14</sup> These anisotropic properties provide researchers one more degree of freedom to design and fabricate high-performance and even novel devices.<sup>15,16</sup> In particular, optical anisotropy

promises the low-symmetry 2D materials to be outstanding candidates for creating diverse angle-dependent optical and optoelectronic devices.<sup>3,4,6–8,16–18</sup> Meanwhile, intrinsic optical anisotropy is a valuable probe for studying the fundamental properties of materials, *e.g.* film thickness, crystalline orientation, and surface and interface modulation, *e.g.* surface oxidation and strain modulation. In this respect, spectroscopy techniques, including optical absorption/reflection,<sup>15,18,19</sup> photoluminescence<sup>20,21</sup> and Raman scattering,<sup>3,20,22</sup> have proven to be powerful tools by disclosing the light–matter interactions. Angle-resolved Raman spectroscopy is widely used to exploit polarization-dependent behaviors, phonons and their coupling to electrons, but it is hard to quantify the anisotropy, considering that the Raman intensity is dependent on the laser power and excitation wavelengths. Despite the wide study of optical anisotropy of low-symmetry 2D materials, the quantitative measurement of this key parameter is still a major hurdle.

In contrast to conventional optical absorption/reflection techniques, we proposed a differential optical method, azimuth-dependent reflectance difference microscopy (ADRDM), to quantitatively measure the normalized reflectance difference of two arbitrary orthogonal directions at normal incidence. This method allows the direct and accurate

<sup>a</sup>State Key Laboratory of Precision Measuring Technology and Instruments, Tianjin University, No. 92 Weijin Road, CN-300072 Tianjin, China. E-mail: cghu@tju.edu.cn

<sup>b</sup>Changchun Institute of Optics and Fine Mechanics and Physics, Chinese Academy of Science, No. 3888 Nanhu Road, CN-130033 Changchun, China

<sup>c</sup>Institute of Experimental Physics, Johannes Kepler University Linz, A-4040 Linz, Austria

† Electronic supplementary information (ESI) available: Details of the ADRDM setup, ADRDM images of *h*-BN/BP/SiO<sub>2</sub>/Si, ADRDM images of PDMS/BP/SiO<sub>2</sub>/Si and ADRDM images of WTe<sub>2</sub>. See DOI: 10.1039/c7nr09173g

visualization of the optical anisotropy of low-symmetry 2D materials. The differential algorithm makes it much more sensitive and robust than the ordinary polarized reflectance (transmittance) measurement. Furthermore, it possesses the advantage of isotropic material immunization because the reflectance difference (RD) signal of isotropic films is always zero. This feature helps to characterize anisotropic materials encapsulated in heterostructures.

In this report, two typical anisotropic 2D materials were studied as examples: few-layered BP, representative of a puckered honeycomb crystal structure, and few-layered ReS<sub>2</sub>, representative of a 1T distorted crystal structure. We revealed that the weak optical anisotropies of trilayer and four-layer BPs on 260 nm Si/SiO<sub>2</sub> were only 0.002 and 0.004, respectively, at a wavelength of 600 nm. We also found that the optical anisotropy of the BP/SiO<sub>2</sub>/Si system was strongly modulated by an interference effect, which is issued from the multilayer structure and leads to unusual switches of the strongest reflectivity directions between zigzag (ZZ) and armchair (AC) crystalline axes as the thickness of BP is increased. Similarly, the interference effect also perturbs the analyses of Raman spectroscopy when polarization-dependent Raman spectroscopy (ADRS) is applied to identify the crystalline orientation of BP, and its data processing is complicated as both the electron-photon (interference effect) and electron-phonon (lattice dynamics) interactions are involved.<sup>19,23</sup> Recently, S. Zhang *et al.* reported a method that identifies the crystalline orientation of BP by measuring the changes of the Raman shifts while applying in-plane uniaxial strain on BP. This method eliminates the crystalline uncertainty between ZZ and AC directions but is limited by the flexibility of the substrate.<sup>24</sup> The optical method (reflection/transmission) in the visible regime is considered as a simpler method to index the crystalline orientation of BP because only the electron-photon interactions are involved. To deal with the interference effect, we applied a scattering matrix method to numerically account for the optical interference and then concluded on the crystalline orientation of BP without the thickness limit. The results were further confirmed using an angle-dependent conductance measurement. Additionally, taking the advantage of ADRDM being insensitive to the optically isotropic layer, we successfully characterized the optical anisotropy of BP encapsulated by a 6 nm hexagonal boron nitride (*h*-BN) sheet. Also the optical anisotropy of ReS<sub>2</sub> was characterized using ADRDM, which demonstrates the capability of ADRDM to index the in-plane crystalline orientations of other anisotropic 2D materials. Our method provides a new *in situ* and nondestructive way to characterize and evaluate anisotropic 2D crystals during various procedures of materials growth, device fabrication and antioxidant protection.

## Results and discussion

Fig. 1a illustrates the optical birefringence of layered BP.<sup>4,15,25</sup> The sp<sup>3</sup> hybridization results in a ridged structure along the

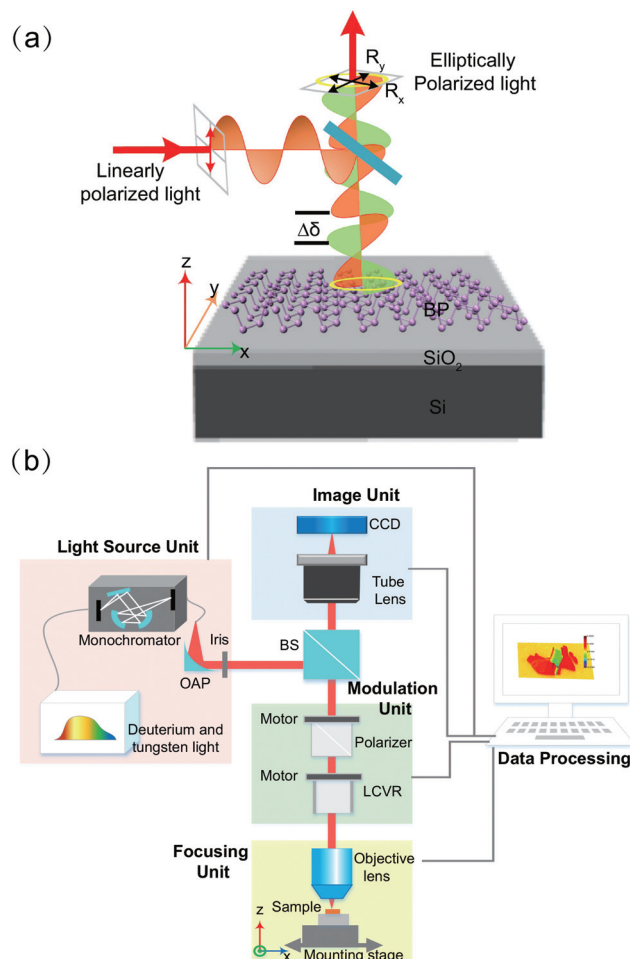


**Fig. 1** (a) Scheme of the birefringence effect in the BP crystal; *x* and *y* denote the armchair and zigzag crystalline orientations, respectively. (b) Scheme of azimuth-dependent reflectance difference microscopy (ADRDM).

ZZ crystalline direction and a puckered structure along the AC crystalline direction, which is shown in the top view of the atomic structure of BP in Fig. 1a.<sup>26</sup> The low-symmetry structure leads to a strong in-plane anisotropic property and the biggest difference of the optical complex indices along the two crystalline axes. When a linearly polarized light is normally incident on the BP crystal, the anisotropic nature of BP gives rise to notable phase retardance ( $\Delta\delta$ ) and reflectance difference ( $\Delta R$ ) between the two optical axes,<sup>25</sup> resulting in elliptically polarized reflectance with unequal reflectance along *x* ( $R_x$ ) and *y* axes ( $R_y$ ). The optical reflectance difference (RD) is defined as:<sup>27,28</sup>

$$\frac{\Delta R}{R} = 2 \frac{R_x - R_y}{R_x + R_y} \quad (1)$$

where *x* and *y* are the coordinate system of the measurement setup. As shown in Fig. 1a,  $\Delta R/R$  reaches an extreme value when the two optical eigen-axes of the sample match the

instrumental axes. The RD technique has been demonstrated by a large number of research studies as a versatile and powerful tool for the characterization of the surfaces and interfaces of semiconductors, including atomic and electronic structures, morphology of surface, doping and surface strain.<sup>28–30</sup> However, the conventional RD approaches are no longer suitable for the measurement of 2D materials because of the extremely tiny size of the 2D flake obtained from mechanical or liquid phase exfoliation.<sup>31,32</sup> Besides, in order to suppress the parasitic ellipsometry, originating from an oblique incidence of light to the isotropic layers, and make sure that the measured RD signal purely comes from the anisotropic 2D sheet, the incident angle of the light beam should be nearly perpendicular to the sample surface,<sup>33,34</sup> which excludes the usage of a high-magnification objective to focus the light spot on the small size samples.

In order to resolve the optical anisotropy  $\Delta R/R$  of the tiny 2D flakes, we developed azimuth-dependent reflectance difference microscopy (ADRDM) based on a liquid crystal variable retarder (LCVR).<sup>35</sup> This electro-photon modulation technique avoided mechanical errors since no optical element was mechanically rotated or moved during the measurement and ensured a high signal-to-noise ratio to our setup. To keep the light incidence angle close to perpendicular, a 5 $\times$  objective lens (Nikon, 5 $\times$ , NA 0.15) and a plane array CCD camera (Apogee, AltaU2) were used in our setup. The 5 $\times$  objective lens converged the light beam from the millimeter scale into a sub-millimeter size spot (incident angle  $\sim 8^\circ$ ) on the sample. Then, the whole field of view was imaged onto a CCD camera. The acquired image was decomposed within an area of 150  $\times$  150 pixels and a lateral resolution of 3  $\mu\text{m}$  was realized. The schematic diagram of the ADRDM setup is shown in Fig. 1b and the details of the setup are provided in ESI section S1.†

For an anisotropic sample with arbitrary azimuthal orientation, the azimuth-dependent RDM (ADRDM) signal can be written as:<sup>36,37</sup>

$$S(\theta) = \Delta R/R_{za} \cos 2(\theta - \theta_0), \quad (2)$$

where  $\Delta R/R_{za} = 2(R_{ZZ} - R_{AC})/(R_{ZZ} + R_{AC})$ ,  $R_{ZZ}$  and  $R_{AC}$  are the reflectance along ZZ and AC directions of BP, respectively.  $\theta$  denotes the azimuthal angles of the incident light and  $\theta_0$  points out the ZZ direction of the sample. Therefore, the optical eigen-axes of the anisotropic film are unambiguously ascertained by plotting  $\Delta R/R$  as a function of the incident azimuthal angle  $\theta$  and then finding the extreme values of the data. According to eqn (2), the azimuthal directions corresponding to the local maximum and minimum RD signals are assigned along with the high and low reflectance axes of the BP film, respectively. Considering the same crystalline orientations of BP for all wavelengths in the visible regime<sup>15</sup> and a high signal-to-noise ratio of the ADRDM setup at a wavelength of 600 nm, we performed all measurements at excitation wavelength of 600 nm as an example in this work for optimal signal quality.

Fig. 2a exhibits a typical optical image (OM) of exfoliated BP on the Si/SiO<sub>2</sub> substrate. Two regions can be roughly distinguished and labeled as zones a and b for simplicity. The average height of zone a is around 2 nm ( $\sim 3$  layers) and zone b is around 3 nm ( $\sim 4$  layers), measured by atomic force microscopy (AFM) (Fig. 2b). We rotated the azimuthal angle from 0° to 345° with an increment of 15° and the minimum RD signal occurred at around  $\theta = 210^\circ$  (Fig. 2c). To study quantitatively the optical anisotropy of the trilayer BP on the Si/SiO<sub>2</sub> substrate, the height information, measured by AFM, and the RD signal along the blue line in Fig. 2c are shown in the upper and lower panels of Fig. 2d, respectively. It reveals that the optical differences of trilayer and four-layer BPs on Si/SiO<sub>2</sub> are only 0.002 and 0.004 at a wavelength of 600 nm ( $\sim 2.06$  eV). They are smaller than those of suspended BP flakes. The calculated RD values of suspended BP are provided in ESI section S2.† This weak anisotropy can be easily understood since the optical gaps of trilayer and four-layer BPs are less than 1 eV (ref. 21) and the absorption of few-layered BP in the visible range is weak. As a result, the BP film contributes small reflectance to the overall reflectance, which is mainly from the Si/SiO<sub>2</sub> substrate. If we treat BP/SiO<sub>2</sub>/Si as an integral, these results indicate that the overall optical anisotropy of the BP/SiO<sub>2</sub>/Si system is modulated by the substrate, even though the substrate is isotropic. It should be noted that the high-symmetrical axes of the BP/SiO<sub>2</sub>/Si system are in line with the crystalline axes of BP (ZZ or AC directions). The obvious difference between 2 nm and 3 nm BP flakes (2d) indicates that the present ADRDM is sensitive enough to discriminate the thickness of BP with monolayer resolution ( $\sim 0.53$  nm for monolayer<sup>3</sup>).

The  $\Delta R/R$  values of both zones a and b are plotted in Fig. 2e and f, respectively, as a function of the azimuthal angle  $\theta$  of the incident light. They are periodic cosine function dependent. Two extreme axes were observed at  $\sim 115^\circ$  (maximum) and  $\sim 205^\circ$  (minimum), respectively, with an angle space of 90°. Fig. 2g depicts all RDM images at different angles in a color scale. Although the optical reflectances of trilayer and four-layer BPs along the ZZ and AC directions have been theoretically calculated,<sup>4,5</sup> the interference effect between interfaces, which disturbs the amplitude of the RD signal, must be taken into account as well when the BP sheet is placed on a multilayer substrate, like SiO<sub>2</sub>/Si. It is a common problem for all optical measurement methods. A totally reversed result induced by an interference effect might be observed when applying angle-resolved Raman spectroscopy to specify the crystalline orientation of the BP flake.<sup>19,23,38</sup>

To explore the interference effect on the optical anisotropy of BP, we present a four-phase model to numerically calculate the nominal optical anisotropy through the method of scattering matrices, which describes quantitatively the total reflection, refraction and transmission of a multilayer system.<sup>39</sup> In the four-phase model of air/BP/SiO<sub>2</sub>/Si (Fig. 3a), the BP flake and SiO<sub>2</sub> layer were treated as thin slabs with certain refractive and absorption coefficients and the Si substrate was regarded as semi-infinite bulk.

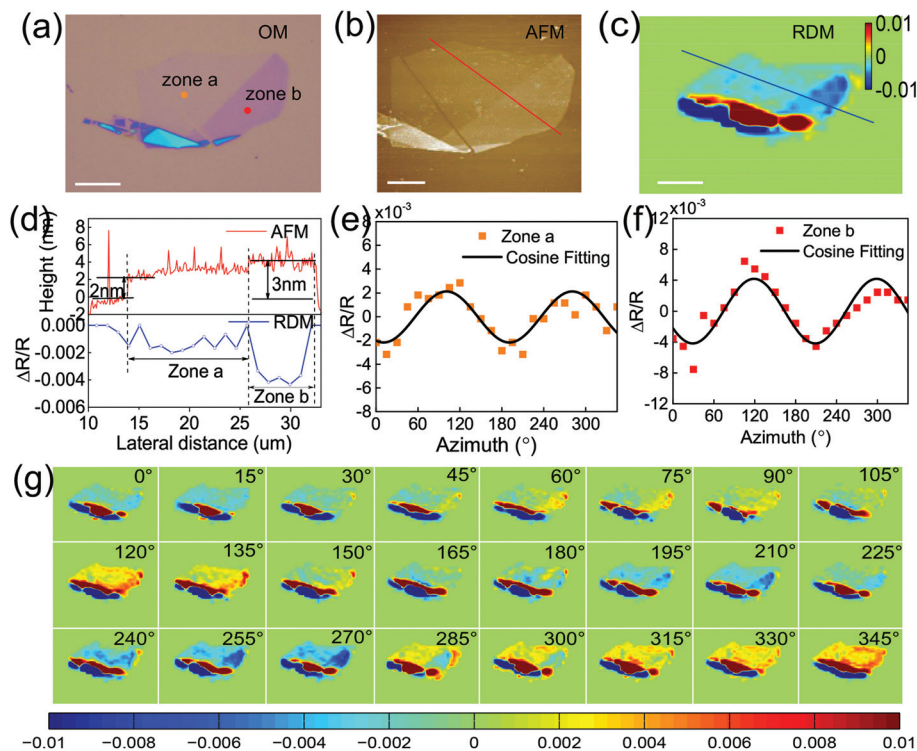


**Fig. 2** (a) Optical image of a BP flake on the Si/SiO<sub>2</sub> substrate. Two different regions are roughly recognized by color and labeled as zone a and zone b. The orange and red circles highlight the positions for ADRDM analysis in (e)–(f). (b) Topography image of the BP sample by AFM. The average heights of zone a and zone b are 2 nm and 3 nm, respectively. (c)  $\Delta R/R$  image taken from the ADRDM measurement at  $\theta = 210^\circ$ . Scale-bar: 5  $\mu\text{m}$ . (d) The upper panel depicts the topographic profile of BP along the red line shown in (b). The lower panel presents the RDM profile along the blue line drawn in (c). (e) Azimuth-dependent  $\Delta R/R_s$  of zone a. (f) Azimuth-dependent  $\Delta R/R_s$  of zone b. (g) All azimuth-dependent RDM images.

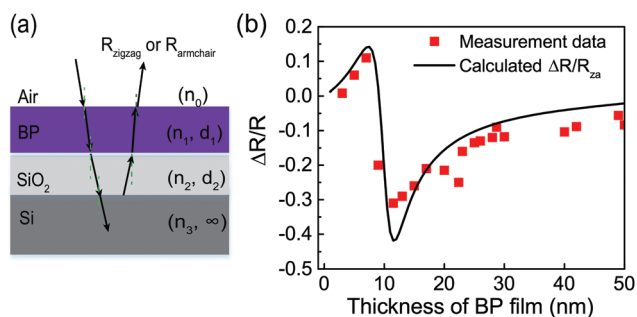


**Fig. 3** (a) Scheme of the four-phase model of the air/BP/SiO<sub>2</sub>/Si sample. (b) Experimental vs. calculated data of the optical anisotropy as a function of the thickness of BP. BP flakes were placed on a 260 nm thermal oxidized silicon covered silicon substrate.

The following special treatments were carried out here to simplify the calculation. First, the incident light can be treated as having a truly normal incidence due to the use of a 5 $\times$  magnification objective in the ADRDM setup.<sup>33</sup> Second, the extreme RD signal corresponds to the case that one of the principal axes of BP is normal or parallel to the plane of the incidence and the incident polarized electric fields parallel to the sample plane, in which the coupling of the s (electric-field

vector  $E$  perpendicular to the plane of incidence) and p ( $E$  parallel to the plane of incidence) polarized light is out of consideration. Therefore, the reflections and absorptions of the s and p components are calculated independently.<sup>15,39</sup> This allows us to separately calculate the reflectances along ZZ and AC directions with their corresponding complex refractive indices.

A total scattering matrix  $S^p$  along the principal axis of the air/BP/SiO<sub>2</sub>/Si system is calculated by:

$$S^p = I_{01}^p \cdot L_1^p \cdot I_{12}^p \cdot L_2^p \cdot I_{23}^p, \quad (3)$$

where p indicates one of the ZZ and AC directions,  $I^p$  and  $L^p$  are the interface and layer matrices, respectively,

$$I_{(m-1)m}^p = \frac{1}{t_{(m-1)m}^p} \begin{pmatrix} 1 & r_{(m-1)m}^p \\ r_{(m-1)m}^p & 1 \end{pmatrix}, \quad (4)$$

and

$$L_m^p = \begin{pmatrix} e^{i\beta_m^p} & 0 \\ 0 & e^{-i\beta_m^p} \end{pmatrix}. \quad (5)$$

Here,  $r_{(m-1)m}^p$  and  $t_{(m-1)m}^p$  are the reflection and transmission coefficients from layer  $(m-1)$  to layer  $(m)$ .  $\beta_m^p$  is the phase shift induced by layer  $m$  ( $m = 1, 2, 3$  and 4). For an inci-

dent light perpendicular to the sample surface, the reflectance coefficients are

$$\begin{aligned} r_{(m-1)m}^p &= \frac{n_{m-1}^p - n_m^p}{n_{m-1}^p + n_m^p}, \\ t_{(m-1)m}^p &= \frac{2n_{m-1}^p}{n_{m-1}^p + n_m^p}, \\ \beta_m^p &= \frac{2\pi d_m n_m^p}{\lambda}, \end{aligned} \quad (6)$$

where  $n_m^p$  and  $d_m^p$  are the complex indices of refraction and the thickness of layer  $m$ , respectively.  $\lambda$  corresponds to the wavelength.

The overall reflection and transmission coefficients of the stratified system are

$$r_p = \frac{S_{21}^p}{S_{11}^p}, \quad t_p = \frac{1}{S_{11}^p}. \quad (7)$$

Therefore, the reflection coefficients along two principal axes of an air/BP/SiO<sub>2</sub>/Si system are given by

$$r_{ZZ} = \frac{S_{21}^{ZZ}}{S_{11}^{ZZ}}, \quad r_{AC} = \frac{S_{21}^{AC}}{S_{11}^{AC}}. \quad (8)$$

The total reflectance intensity ( $R_{ZZ}$  or  $R_{AC}$ ) is obtained through multiplying the reflected beam amplitude by its complex conjugate.<sup>40</sup> Using eqn (3)–(8), we calculate  $\Delta R/R_{za}$  of few-layer BP on the SiO<sub>2</sub>/Si substrate. The complex refractive indexes of BP ( $n_1$ ) were taken from N. Mao, *et al.*<sup>15</sup> and the refractive indexes of SiO<sub>2</sub> ( $n_2$ ) and Si ( $n_3$ ) were taken from Palik, *et al.*<sup>41</sup> The thickness of SiO<sub>2</sub> was 260 nm as measured by spectroscopic ellipsometry (J. A. Woollam, M2000).

The solid black line in Fig. 3b exhibits the calculated  $\Delta R/R_{za}$  of BP on the SiO<sub>2</sub>/Si substrate as a function of the thickness of the BP film. To verify our calculation, we carried out ADRDM measurements on a series of BP flakes with different thicknesses, which were determined by AFM, and the experimental data were presented by the red discrete squares in Fig. 3b. The calculation results are consistent with the experimental data except for a slight divergence. It might be caused by surface oxidization, thickness offset and even refractive index variation with an increase in the thickness of the BP flake due to the possible changes of physical properties of BP.<sup>42</sup>

Numerical simulation (Fig. 3b) implies that the interference effect of the multilayer structure of BP/SiO<sub>2</sub>/Si non-linearly tunes the nominal optical anisotropy of BP, which in fact depends on the thicknesses of BP and SiO<sub>2</sub>. A similar effect on the Raman spectroscopy of graphene on SiO<sub>2</sub> has already been systematically discussed.<sup>38,43</sup> But the interference effect on the optical anisotropy of BP has not been reported yet. Here, we focus on how the interference affects the optical anisotropy with an increase in the thickness of BP since the interference problem is common for optical methods in the characterization of 2D materials. When the substrate is 260 nm thermal oxidized silicon on silicon, we note that the  $\Delta R/R$  increases with the BP thickness from 1 nm to 7 nm, which peaks at

~7 nm, and then a switch of high and low reflectance axes between ZZ and AC directions occurs at a thickness around ~8 nm. We conclude that the reflectance along the ZZ direction is larger than that of the AC direction when the thickness of BP is less than 8 nm. In contrast, the reflectance along the AC direction is larger than that of the ZZ direction when the thickness of BP varies from 8 nm to 50 nm. Comparing this result with preceding work which concludes from a DFT analysis that the optical absorption along the AC direction should be larger than the one along the ZZ direction in the visible range for all flake thicknesses,<sup>23</sup> we believe that this observed switch originates from the light interference effect.

In order to further solidify this switch, we conducted angle-resolved conductance measurement on a 10 nm BP flake to identify its crystalline orientation. In the measurement, we first applied ADRDM to determine the directions of two crystalline axes of the sample. Fig. 4a shows the ADRDM images taken at different azimuthal angles. To minimize the exposure of BP flakes to air, we reduced the angular range of  $\theta$  to (0°–90°) with a resolution of 15° and then used a cosine fitting to determine the lattice orientations. Fig. 4b shows the  $\Delta R/R$  data versus the azimuthal angles, in which the extreme  $\Delta R/R$  at  $\theta_0 = 38^\circ$  is determined by the fitting process. The insert in Fig. 4b displays the OM and AFM images. We carried out AFM measurement in a small region highlighted by a white rectangle in the OM image to avoid long time air exposure of

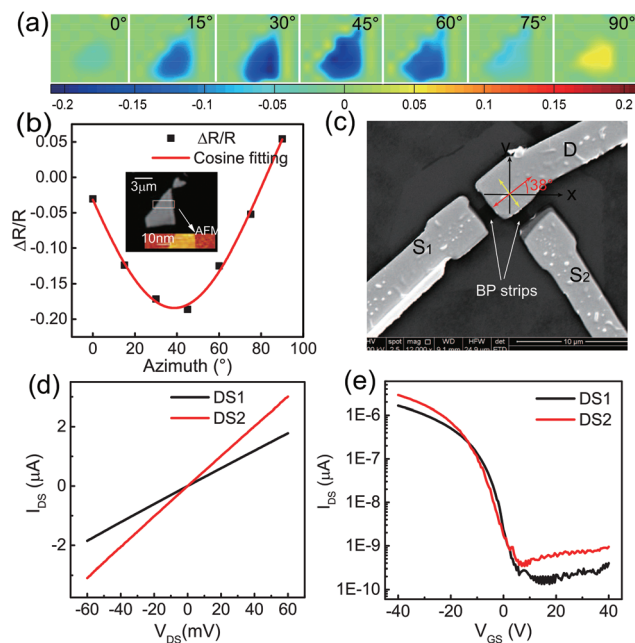


**Fig. 4** (a) ADRDM images taken at different azimuthal angles. Scale-bar: 3  $\mu\text{m}$ . (b)  $\Delta R/R$  varies with the azimuthal angles of the polarized incident light. Insert: Optical image and AFM images taken from the region indicated as the white rectangle. The thickness of the BP flake is 10 nm. (c) SEM image of fabricated BP strips with metal electrodes patterned at the specific orientations determined by ADRDM measurement. (d)  $I$ - $V$  curves of the two orthogonal BP flakes at  $V_{GS} = -40$  V. (e) The transfer characteristics of the two BP strips at  $V_{DS} = 50$  mV.

BP. The thickness of BP is about 10 nm. With the ADRDM results, the BP flake was shaped into a strip shape along the two extreme  $\Delta R/R$  directions of  $\theta_{01} = 38^\circ$  and  $\theta_{02} = 128^\circ$ . The fabrication process has been reported in our previous research.<sup>44</sup>

Fig. 4c shows the image of the two patterned BP strips with metal electrodes obtained using a scanning electron microscope (SEM). Fig. 4d shows the  $I$ - $V$  measurements of the two BP devices and both BP strips (labelled as DS<sub>1</sub> and DS<sub>2</sub>) were negatively biased at  $V_{GS} = -40$  V by the back gate. The derived conductances of DS<sub>1</sub> and DS<sub>2</sub> are 30.20 and 50.85  $\mu$ S from the linear  $I$ - $V$  curves, which corresponds to a conductance anisotropy (defined as  $2(G_x - G_y)/(G_x + G_y)$ ,  $G_x$  and  $G_y$  being the conductances along the two orthogonal directions) of  $\sim 50.9\%$ , which agree well with a previous report.<sup>2</sup> Considering the extreme anisotropy of 50.9% between the two orthogonal directions, we assumed that DS<sub>1</sub> and DS<sub>2</sub> are nearly aligned along the principal axes of the BP flake. Fig. 4e shows the transfer characteristic of the two BP devices at  $V_{DS} = 50$  mV with a gate bias scanning from  $-40$  V to 40 V, which indicates a current on/off ratio of  $\sim 10^4$ . According to the conductance measurement, we ascertain that the two BP strips, DS<sub>1</sub> and DS<sub>2</sub>, are aligned along the ZZ and AC directions, since both the theoretical and experimental results indicate that the electron and hole mobilities of BP along the AC directions are higher than that along the ZZ direction.<sup>4</sup> This result confirms that the local maximum and minimum ADRDM of 10 nm BP corresponds to the AC and ZZ direction, respectively, and is consistent with our theory presented above.

As the switch of high and low reflectances along two crystal orientations is clearly demonstrated, our results establish a special caution for light interference when using optical methods to specify the exact crystalline orientations. In practice, such an interference effect is inevitable for optical measurement. To deal with it, we developed the multi-phase model based on the method of scattering matrices to calculate reflectances along the principal axes and it has been proved to be feasible. Moreover, one advantage of the calculation method is that if the number of layers of the film system increases, one just need to multiply the corresponding scattering matrices of these layers to obtain the overall scattering matrix of the film system.<sup>45</sup> This feature makes the method highly convenient for calculating  $\Delta R/R$  of a multilayer hetero-structure. Associated with the calculation method, ADRDM is a powerful tool to identify the crystalline orientation when the thickness of a sample is roughly estimated. Fortunately, an ordinary optical microscope can be used to estimate the thickness of a BP flake with the naked eye by judging the sample's color after a simple calibration procedure of the optical microscope setup.<sup>46</sup>

In order to overcome the degradation of BP in air, sandwiched BP structures, including encapsulation by atomic-thick  $\text{Al}_2\text{O}_3$ <sup>47–49</sup> and BP-based hetero-structures,<sup>50–53</sup> have drawn huge attention. Identifying the crystalline orientation of capped BP will be of great benefit for utilizing the outstanding anisotropy to build polar hetero-devices. However, a top layer

on the BP flake demands more rigorous and complicated measurements. Interestingly, the top isotropic layers have in principle no contribution to the differential reflectance  $\Delta R$ , which makes ADRDM extremely suitable for *in situ* indexing the principal axes of capped BP, as compared to other optical approaches.

We conducted ADRDM measurement on an *h*-BN-BP hetero-structure as an example. Fig. 5a depicts the scheme of an air/*h*-BN/BP/SiO<sub>2</sub>/Si system. In experiment, we first exfoliated few-layered BP on a Si/SiO<sub>2</sub> substrate and then carried out the ADRDM measurement to determine the principal axes of pristine BP. After that, a 6 nm *h*-BN layer was exfoliated and used to cap the BP flake, whose thickness was confirmed by AFM (Fig. 5b). The thickness of the thicker part of BP is around 22 nm derived from AFM. Fig. 5c depicts the OM and RDM images of the bare (upper panel) and capped BP (lower panel) at  $\theta_0 = 30^\circ$  and the corresponding  $\Delta R/R$  of the selected section. The ADRDM gives a positive maximum at  $\theta_0 = 30^\circ$ , which indicates the AC direction. All ADRDM images with an incident azimuthal angle from  $0^\circ$  to  $180^\circ$  with an angular resolution of  $30^\circ$  are presented in ESI section S3.†

In Fig. 5c, zones a and b highlighted in the OM are clearly distinguished in the RDM images no matter the BP flake is bare or covered and only a small amplitude difference of  $\Delta R/R$  exists between the two RDM images. This demonstrates the capability of ADRDM to directly visualize the distribution of optical anisotropy of a covered BP flake. The slight amplitude

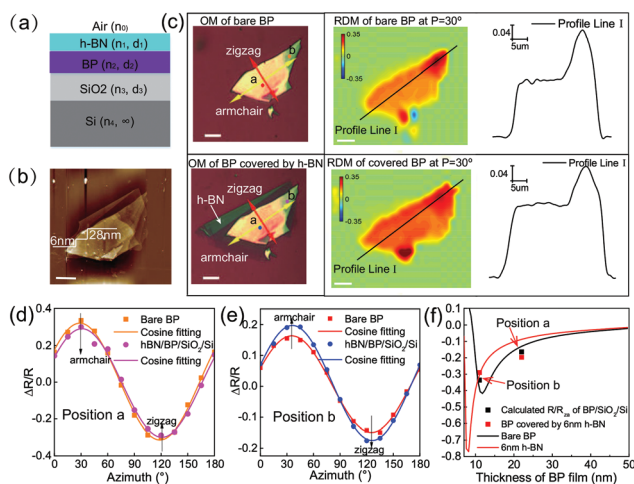
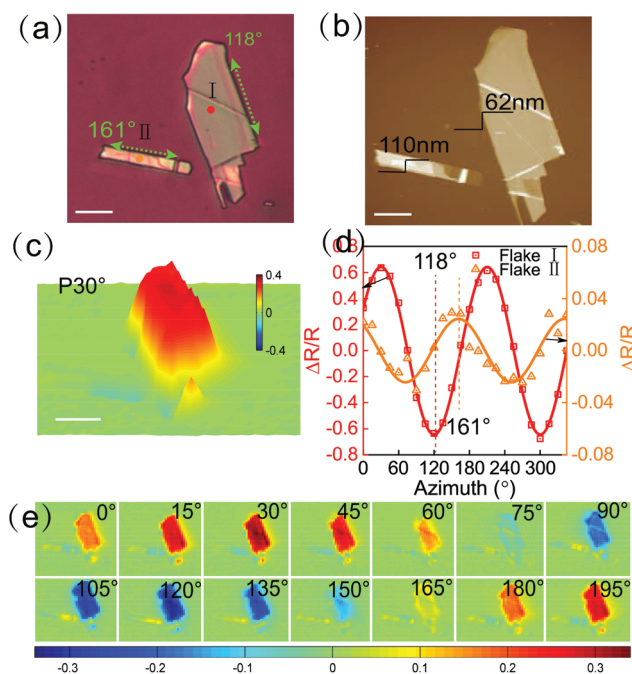


Fig. 5 (a) Scheme of an *h*-BN/BP/SiO<sub>2</sub>/Si structure. (b) AFM image of the sample covered by a 6 nm *h*-BN layer. The height of the thick part is around 22 nm. (c) RDM images of the bare and covered BP samples at the incident polarization of  $\theta = 30^\circ$ . Two arrows sketched in the OM indicate the crystalline orientations determined by the later ADRDM measurement. Scale-bar: 5  $\mu$ m. (d)  $\Delta R/R$  extracted from the position a as a function of azimuthal angles. The red squares and blue circles represent the results taken from the BP flake before and after covered by the *h*-BN layer, respectively. The corresponding solid lines are the cosine function fitting curves. (e)  $\Delta R/R$  varies with the azimuthal angles at position b. (f) The solid lines indicate the simulated  $\Delta R/R_{2a}$  of bare and *h*-BN-capped BP as a function of the thickness of BP. The scattered squares indicate the experimental data.

change of  $\Delta R/R$  can be easily understood recalling that the isotropic layer will contribute to the entire reflectance  $R$  of the system and have no contribution to the differential reflectance  $\Delta R$ . The exact ADRDM value of the capped sample can be estimated by  $S(\theta) = (\Delta R/R + \alpha)\cos 2(\theta - \theta_0)$ , where  $\alpha$  is the amplitude change caused by the top isotropic layer in the direction where the incident polarization parallel to one of the optical eigen-axes of the sample. Apparently, the homogeneously isotropic layer has no influence for indexing the orientations of the anisotropic samples. Therefore, the ADRDM is an effective tool to identify the crystalline orientation of the covered BP flakes. Fig. 5d and e are the plots of the  $\Delta R/R_s$  of regions a and b as a function of the incident azimuthal angle  $\theta$ . The measured crystalline orientation did not change at all before and after the BP flake was covered. We also confirmed that the ADRDM was able to identify the principle axes of BP flakes capped with a PDMS film which is much thicker than the BP flake and the results are presented in ESI section S4.†

We calculated  $\Delta R/R_{za}$  of BP covered by the 6 nm *h*-BN film. The value of  $n_0 = 2.13$  has been taken from ref. 54 for the ordinary refractive index perpendicular to the direction of light propagation. The red solid line in Fig. 5f depicts the calculated  $\Delta R/R_{za}$  of a sample of air/*h*-BN/BP/SiO<sub>2</sub>/Si varying with the thickness of BP and the scattered squares point out the measured data. The black solid line indicates the calculation result for bare BP on the Si/SiO<sub>2</sub> substrate. A slight divergence between the simulation results and measured data exists; it could be due to the fact that the *h*-BN layer did not stick closely enough onto the BP flake and an air gap exists between the *h*-BN film and the BP flake.

Apart from BP, we also applied the ADRDM technique to characterize triclinic layered ReS<sub>2</sub>, a typical representative of another class of anisotropic 2D crystals with a 1T distorted structure, whose anisotropy has been studied in a number of reports.<sup>6–8</sup> Fig. 6a exhibits a typical optical image of three ReS<sub>2</sub> flakes on the Si/SiO<sub>2</sub> substrate. The green dashed arrows in OM indicate the *b*-axes of each flake, which is judged from the clear and sharp edges of the sample.<sup>55</sup> The thicknesses of flake I and flake II are 62 nm and 109 nm, respectively, from the AFM image in Fig. 6b. Fig. 6c shows a view of the optical anisotropies of three flakes taken at angle  $\theta = 30^\circ$ . Two flakes have an obvious difference in optical anisotropy. Fig. 6d shows the azimuth dependent  $\Delta R/R_s$  of flakes I and II under an excitation wavelength of 600 nm, which reveals the orientation differences of the two samples. Fig. 6e shows a montage of ADRDM images taken at different azimuthal angles. Accurate values for the refractive indices of few-layered ReS<sub>2</sub> are required in order to discriminate the specific AC/ZZ orientation of the samples,<sup>55</sup> but unfortunately these data are not yet available in the literature. As a matter of fact, the RDM has a potential to derive the complex refractive indices of the sample using wavelength scanning measurement.<sup>56,57</sup> Furthermore, we found that flake I has a very strong optical anisotropy  $\Delta R/R$  of 0.62 while flake II has a relatively weak  $\Delta R/R$  of 0.038. We believe that the difference of  $\Delta R/R_s$  is also induced by the optical tuning of the interference effect,



**Fig. 6** (a) Optical image of ReS<sub>2</sub> on the Si/SiO<sub>2</sub> substrate. (b) AFM image of flakes I and II. Scale bar: 10  $\mu$ m. (c) RDM image at an azimuthal angle of 30°. Scale-bar: 10  $\mu$ m. (d) Azimuth-resolved anisotropy of flake I and flake II. (e) ADRDM images at different azimuthal angles.

similar to the situation of BP characterization. Indeed, such a strong optical anisotropy is not expected for pristine ReS<sub>2</sub>. We also used the ADRDM setup to evaluate the optical anisotropy of WTe<sub>2</sub> and the results are presented in ESI section S5.† All the measurement results suggest that the ADRDM is a powerful tool to visualize the optical anisotropy and explore the interference effect of a multilayer structure even though some of the layers are of nanometer thickness. We believe that the proposed ADRDM is of great benefit for investigation on and applications of anisotropic 2D materials.

## Conclusions

In conclusion, we proposed a differential optical approach to accurately resolve the optical anisotropy of anisotropic 2D materials in a nondestructive and space-resolved manner. The imaging technique enables one to visualize the local distribution of the optical anisotropy of samples without any perturbation due to the presence of isotropic layers above or below the samples. This optical method is also capable of probing the thickness of BP with monolayer resolution. In order to issue the multilayer-induced interference disturbance to the optical anisotropy measurement, an effective numerical model based on the method of the scattering matrices was developed. With both experimental and theoretical investigations, the modulation of the interference effect on the optical anisotropy of BP flakes was clearly revealed. Furthermore, our approach provides a simple and effective way to identify *in situ* crystal-

line orientations of both bare and encapsulated samples, which is a big deal for further investigations and applications of BP and ReS<sub>2</sub>. This technique can be widely applied to quantify the optical nature of other anisotropic nanometer-thick crystals and characterize their crystalline axes.

## Conflicts of interest

There are no conflicts to declare.

## Acknowledgements

The authors thank Dr Matthias Duwe at Accurion company, Prof. Wei Ji, Dr Feng Yang and Dr Jingsi Qiao at Renmin University of China for the discussions of refractive indices of few-layered BP. This work was funded by the National Natural Science Foundation of China (NSFC) (Grant No. 61008028), the National Key Research and Development Program (Grant No. 2016YFB1102203, 2017YFF0107003) and the 111 Project of China (Grant No. B07014).

## References

- L. Li, Y. Yu, G. J. Ye, Q. Ge, X. Ou, H. Wu, D. Feng, X. H. Chen and Y. Zhang, *Nat. Nanotechnol.*, 2014, **9**, 372–377.
- H. Liu, A. T. Neal, Z. Zhu, Z. Luo, X. Xu, D. Tománek and P. D. Ye, *ACS Nano*, 2014, **8**, 4033–4041.
- F. Xia, H. Wang and Y. Jia, *Nat. Commun.*, 2014, **5**, 4458.
- J. Qiao, X. Kong, Z.-X. Hu, F. Yang and W. Ji, *Nat. Commun.*, 2014, **5**, 4475.
- V. Tran, R. Soklaski, Y. Liang and L. Yang, *Phys. Rev. B: Condens. Matter*, 2014, **89**, 235319.
- E. Liu, Y. Fu, Y. Wang, Y. Feng, H. Liu, X. Wan, W. Zhou, B. Wang, L. Shao, C.-H. Ho, Y.-S. Huang, Z. Cao, L. Wang, A. Li, J. Zeng, F. Song, X. Wang, Y. Shi, H. Yuan, H. Y. Hwang, Y. Cui, F. Miao and D. Xing, *Nat. Commun.*, 2015, **6**, 6991.
- D. A. Chenet, O. B. Aslan, P. Y. Huang, C. Fan, A. M. van der Zande, T. F. Heinz and J. C. Hone, *Nano Lett.*, 2015, **15**, 5667–5672.
- O. B. Aslan, D. A. Chenet, A. M. van der Zande, J. C. Hone and T. F. Heinz, *ACS Photonics*, 2015, **3**, 96–101.
- Q. Song, X. Pan, H. Wang, K. Zhang, Q. Tan, P. Li, Y. Wan, Y. Wang, X. Xu, M. Lin, X. Wan, F. Song and L. Dai, *Sci. Rep.*, 2016, **6**, 29254.
- E. Torun, H. Sahin, S. Cahangirov, A. Rubio and F. Peeters, *J. Appl. Phys.*, 2016, **119**, 074307.
- K. S. Novoselov, A. K. Geim, S. V. Morozov, D. Jiang, Y. Zhang, S. V. Dubonos, I. V. Grigorieva and A. A. Firsov, *Science*, 2004, **306**, 666–669.
- K. Novoselov, D. Jiang, F. Schedin, T. Booth, V. Khotkevich, S. Morozov and A. Geim, *Proc. Natl. Acad. Sci. U. S. A.*, 2005, **102**, 10451–10453.
- Q. H. Wang, K. Kalantar-Zadeh, A. Kis, J. N. Coleman and M. S. Strano, *Nat. Nanotechnol.*, 2012, **7**, 699–712.
- X. Wang and S. Lan, *Adv. Opt. Photonics*, 2016, **8**, 618–655.
- N. Mao, J. Tang, L. Xie, J. Wu, B. Han, J. Lin, S. Deng, W. Ji, H. Xu, K. Liu, L. Tong and J. Zhang, *J. Am. Chem. Soc.*, 2016, **138**, 300–305.
- S. Ge, C. Li, Z. Zhang, C. Zhang, Y. Zhang, J. Qiu, Q. Wang, J. Liu, S. Jia, J. Feng and D. Sun, *Nano Lett.*, 2015, **15**, 4650–4656.
- M. Buscema, D. J. Groenendijk, S. I. Blanter, G. A. Steele, H. S. van der Zant and A. Castellanos-Gomez, *Nano Lett.*, 2014, **14**, 3347–3352.
- H. Yuan, X. Liu, F. Afshinmanesh, W. Li, G. Xu, J. Sun, B. Lian, A. G. Curto, G. Ye, Y. Hikita, Z. Shen, S.-C. Zhang, X. Chen, M. Brongersma, H. Y. Hwang and Y. Cui, *Nat. Nanotechnol.*, 2015, **10**, 707–713.
- X. Ling, S. Huang, E. H. Hasdeo, L. Liang, W. M. Parkin, Y. Tatsumi, A. R. Nugraha, A. A. Puzos, P. M. Das, B. G. Sumpter, D. B. Geohegan, J. Kong, R. Saito, M. Drndic, V. Meunier and M. S. Dresselhaus, *Nano Lett.*, 2016, **16**, 2260–2267.
- X. Wang, A. M. Jones, K. L. Seyler, V. Tran, Y. Jia, H. Zhao, H. Wang, L. Yang, X. Xu and F. Xia, *Nat. Nanotechnol.*, 2015, **10**, 517–521.
- J. Yang, R. Xu, J. Pei, Y. W. Myint, F. Wang, Z. Wang, S. Zhang, Z. Yu and Y. Lu, *Nat. Nanotechnol.*, 2015, **4**, e312.
- J. Wu, N. Mao, L. Xie, H. Xu and J. Zhang, *Angew. Chem.*, 2015, **127**, 2396–2399.
- J. Kim, J.-U. Lee, J. Lee, H. J. Park, Z. Lee, C. Lee and H. Cheong, *Nanoscale*, 2015, **7**, 18708–18715.
- S. Zhang, N. Mao, J. Wu, L. Tong, J. Zhang and Z. Liu, *Small*, 2017, **13**, 1700466.
- S. Lan, S. Rodrigues, L. Kang and W. Cai, *ACS Photonics*, 2016, **3**, 1176–1181.
- X. Liu, C. R. Ryder, S. A. Wells and M. C. Hersam, *Small Methods*, 2017, **1**, 1700143.
- J. D. E. McIntyre and D. E. Aspnes, *Surf. Sci.*, 1971, **24**, 417–434.
- D. Aspnes, *J. Vac. Sci. Technol., B: Microelectron. Process. Phenom.*, 1985, **3**, 1498–1506.
- P. Weightman, D. Martin, R. Cole and T. Farrell, *Rep. Prog. Phys.*, 2005, **68**, 1251.
- L. Sun, J. Gall, G. Weidlinger, C. Liu, M. Denk and P. Zeppenfeld, *Phys. Rev. Lett.*, 2013, **110**, 106101.
- P. Yasaei, B. Kumar, T. Foroozan, C. Wang, M. Asadi, D. Tuschel, J. E. Indacochea, R. F. Klie and A. Salehi-Khojin, *Adv. Mater.*, 2015, **27**, 1887–1892.
- A. Castellanos-Gomez, L. Vicarelli, E. Prada, J. O. Island, K. Narasimha-Acharya, S. I. Blanter, D. J. Groenendijk, M. Buscema, G. A. Steele, J. Alvarez, H. W. Zandbergen, J. J. Palacios and H. S. van der Zant, *2D Mater.*, 2014, **1**, 025001.
- O. Acher and B. Drévillon, *Rev. Sci. Instrum.*, 1992, **63**, 5332–5339.

- 34 W. Shen, C. Hu, S. Li and X. Hu, *Appl. Surf. Sci.*, 2017, **421**, 535–541.
- 35 S. Huo, C. Hu, W. Shen, Y. Li, L. Sun and X. Hu, *Appl. Opt.*, 2016, **55**, 9334–9340.
- 36 M. Brinkley, G. Powell and D. Aspnes, *Appl. Phys. Lett.*, 2006, **88**, 202112.
- 37 K. Schmidegg and P. Zeppenfeld, *Appl. Phys. Lett.*, 2007, **90**, 231903.
- 38 D. Yoon, H. Moon, Y.-W. Son, J. S. Choi, B. H. Park, Y. H. Cha, Y. D. Kim and H. Cheong, *Phys. Rev. B: Condens. Matter*, 2009, **80**, 125422.
- 39 R. M. Azzam and N. M. Bashara, *Ellipsometry and polarized light*, North-Holland. sole distributors for the USA and Canada, Elsevier Science Publishing Co., Inc., 1987.
- 40 M. Born and E. Wolf, *Principles of Optics, seventh expanded edition*, Cambridge, England, 1999.
- 41 E. D. Palik, *Handbook of optical constants of solids*, Academic press, 1998, vol. 3.
- 42 R. Schuster, J. Trinckauf, C. Habenicht, M. Knupfer and B. Büchner, *Phys. Rev. Lett.*, 2015, **115**, 026404.
- 43 C. Casiraghi, A. Hartschuh, E. Lidorikis, H. Qian, H. Harutyunyan, T. Gokus, K. Novoselov and A. Ferrari, *Nano Lett.*, 2007, **7**, 2711–2717.
- 44 J. Tao, W. Shen, S. Wu, L. Liu, Z. Feng, C. Wang, C. Hu, P. Yao, H. Zhang, W. Pang, X. Duan, J. Liu, C. Zhou and D. Zhang, *ACS Nano*, 2015, **9**, 11362–11370.
- 45 Y. Li, N. Dong, S. Zhang, K. Wang, L. Zhang and J. Wang, *Nanoscale*, 2016, **8**, 1210–1215.
- 46 H. Li, J. Wu, X. Huang, G. Lu, J. Yang, X. Lu, Q. Xiong and H. Zhang, *ACS Nano*, 2013, **7**, 10344–10353.
- 47 J. Na, Y. T. Lee, J. A. Lim, D. K. Hwang, G.-T. Kim, W. K. Choi and Y.-W. Song, *ACS Nano*, 2014, **8**, 11753–11762.
- 48 J. D. Wood, S. A. Wells, D. Jariwala, K.-S. Chen, E. Cho, V. K. Sangwan, X. Liu, L. J. Lauhon, T. J. Marks and M. C. Hersam, *Nano Lett.*, 2014, **14**, 6964–6970.
- 49 J. Pei, X. Gai, J. Yang, X. Wang, Z. Yu, D.-Y. Choi, B. Luther-Davies and Y. Lu, *Nat. Commun.*, 2016, **7**, 10450.
- 50 X. Chen, Y. Wu, Z. Wu, Y. Han, S. Xu, L. Wang, W. Ye, T. Han, Y. He, Y. Cai and N. Wang, *Nat. Commun.*, 2015, **6**, 7315.
- 51 A. Avsar, I. J. Vera-Marun, J. Y. Tan, K. Watanabe, T. Taniguchi, A. H. Castro Neto and B. Ozyilmaz, *ACS Nano*, 2015, **9**, 4138–4145.
- 52 Y. Cao, A. Mishchenko, G. Yu, E. Khestanova, A. Rooney, E. Prestat, A. Kretinin, P. Blake, M. Shalom, C. Woods, J. Chapman, G. Balakrishnan, I. Grigorieva, K. Novoselov, B. Piot, M. Potemski, K. Watanabe, T. Taniguchi, S. Haigh, A. Geim and R. Gorbachev, *Nano Lett.*, 2015, **15**, 4914–4921.
- 53 G. C. Constantinescu and N. D. Hine, *Nano Lett.*, 2016, **16**, 2586–2594.
- 54 R. Poerschke and O. Madelung, *Data in Science and Technology, Semiconductors, Group IV Elements and III-V Compounds*, Springer-Verlag, Berlin/Marburg, 1991.
- 55 L. Hart, S. Dale, S. Hoyer, J. L. Webb and D. Wolverson, *Nano Lett.*, 2016, **16**, 1381–1386.
- 56 D. Martin and P. Weightman, *Surf. Interface Anal.*, 2001, **31**, 915–926.
- 57 O. Hunderi, J.-T. Zettler and K. Haberland, *Thin Solid Films*, 2005, **472**, 261–269.